Hindawi
International Journal of Polymer Science
Volume 2019, Article ID 9302803, 12 pages
https://doi.org/10.1155/2019/9302803

Research Article

Functionalized Multiwalled Carbon Nanotube-Reinforced Polyimide Composite Films with Enhanced Mechanical and Thermal Properties

Min Chao,[1] **Yanming Li**,[1] **Guanglei Wu**,[2,3] **Zhenjun Zhou**,[1] **and Luke Yan**[1]

[1]*Polymer Materials & Engineering Department, School of Materials Science & Engineering, Engineering Research Center of Transportation Materials, Ministry of Education, Chang'an University, Xi'an 710064, China*
[2]*Institute of Materials for Energy and Environment, State Key Laboratory of Bio-Fibers and Eco-Textiles, College of Materials Science and Engineering, Qingdao University, Qingdao 266071, China*
[3]*Key Laboratory of Engineering Dielectrics and Its Application, Ministry of Education, Harbin University of Science and Technology, Harbin 150080, China*

Correspondence should be addressed to Luke Yan; yanlk_79@hotmail.com

Received 25 April 2019; Accepted 12 June 2019; Published 14 August 2019

Guest Editor: Chao Zhang

Polyimide- (PI-) based nanocomposites containing the 4,4′-diaminodiphenyl ether- (ODA-) modified multiwalled carbon nanotube (MWCNT) filler were successfully prepared. The PI/MWCNTs-ODA composite films exhibit high thermal conductivity and excellent mechanical property. The optimal value of thermal conductivity of the PI/MWCNTs-ODA composite film is 0.4397 W/mK with 3 wt.% filler loading, increased by 221.89% in comparison with that of the pure PI film. In addition, the tensile strength of the PI/MWCNTs-ODA composite film is 141.48 MPa with 3 wt.% filler loading, increased by 20.74% in comparison with that of the pure PI film. This work develops a new strategy to achieve a good balance between the high thermal conductivity and excellent mechanical properties of polyimide composite films by using functionalized carbon nanotubes as an effective thermal conductive filler.

1. Introduction

Polyimide (PI) has been demonstrated one of the most important high-performance engineering plastics for its excellent mechanical property [1–3], thermal stability [4], and chemical resistance [5] because of its rigid-rod chemical structures, showing appealing potential in the area of electronic applications, membrane, insulating materials, and aerospace industry [6–10]. However, the very low thermal conductivity (0.1 W/mK) of PI can hardly meet the thermal requirements of electronic products, which limits its application in advanced microelectronics and aerospace applications. In order to facilitate the heat dissipation, it is necessary to further improve the thermal conductivity of PI. Therefore, improving the thermal conductivity of PI to endow it with better comprehensive performance has become a research focus. Introducing functional groups or elements into the main chain is an effective way to improve the performance of PI by lengthening the molecular chain and reducing the interaction between molecular chains. In addition, adding high thermal conductive fillers is another facile method to promote the thermal performance of PI [11–17].

Various inorganic fillers owning high thermal conductivity have been added into the PI matrix by in situ polymerization to improve the overall performance of PI, including carbon black [18, 19], alumina (Al_2O_3) [20, 21], aluminum nitride (AlN) [22, 23], silica (SiO_2) [24, 25], titanium dioxide (TiO_2) [26], silicon carbide (SiC) [27, 28], silicon nitride (Si_3N_4) [29, 30], boron nitride (BN) [31, 32], and zinc oxide (ZnO) [33, 34]. Compared with the abovementioned inorganic fillers, carbon nanotubes (CNTs) possess high electrical conductivity (10^5 S·cm^{-1}) and thermal conductivity (3500 W/mK) and extremely high Young modulus (0.9 TPa) and tensile strength (150 GPa), as well as

excellent optical properties [35]. So, CNTs are considered to be the most optimal candidate as ideal enhancing fillers in high tensile, light weight polymer nanocomposites [36–41]. Although CNTs have many merits, there are two major disadvantages that limit their reinforcing efficiency: (1) the bad dispersion of nanoparticles in the polymer matrix and (2) the weak interfacial interaction between nanoparticles and polymer matrix [42–44].

Hence, increasing the dispersion of carbon nanotube nanoparticles in the polymer matrix and enhancing the interfacial interaction between nanoparticles and polymer matrix are critical troubles to make carbon nanotubes fully exert their potential to enhance the performance of the polymer matrix. Wang et al. [45] investigated graphene oxide@carbon nanotube- (GO/CNT-) reinforced PI; by the crosslinking between the amide bonds, the dispersibility of the nanoparticles in the polyimide matrix can be improved and the interfacial interaction between the nanoparticles and the PI matrix can be improved. Li et al. [46] reported that multiwalled carbon nanotubes (MWCNTs) were revised by polyacrylic acid, polyacrylamide, or poly(hydroxyethyl methylacrylate) which is used in the field of biomineralization. The polymer chains were deposited on the MWCNTs by photoinitiated polymerization of the monomers. Chen et al. [47] investigated the amine-treated MWCNTs/epoxy composites in which amine-treated MWCNTs were used as curing agents and are covalently grafted into the epoxy matrix. The tensile strength and impact strength of the composites increase with the content of MWCNTs, and the most significant improvement of the tensile strength is obtained with the addition of 1.5 wt.% amine-treated MWCNTs; the thermal stability of the nanocomposites also distinctly improves. In addition, different amine-treated graphenes, including ethylenediamine, diethylenetriamine, and p-phenylenediamine (EG, DG, and PG, respectively), were employed in synthesizing different contents of PI composites by in situ polymerization [48].

In this work, we prepared carboxylated carbon nanotubes; then, the carboxyl treated MWCNTs (MWCNTs-COOH) were reacted with 4,4′-diaminodiphenyl ether (ODA) to obtain the amino carbon nanotubes (MWCNTs-ODA), which is used to synthesize PI composites by in situ polymerization. The PI composite films prepared by this method can improve the compatibility of CNTs with the PI matrix. The mechanical and thermal properties of PI/MWCNTs-ODA nanocomposite films were studied, while varying different contents in the MWCNTs-ODA.

2. Experimental

2.1. Materials. Multiwalled carbon nanotubes (MWCNTs) were obtained from Chengdu Organic Chemicals Co. Ltd., Chinese Academy of Sciences (China), with the length of 10-30 μm; the outer diameter is 10-20 nm and a purity of >98%. Pyromellitic dianhydride (PMDA) (purity: >98.5%) and 4,4′-diaminodiphenyl ether (ODA) (purity: >98.0%) were purchased from Sinopharm Chemical Reagent Co. Ltd., China. N,N-Dimethylacetamide (DMAc) (purity: >99.5%), N,N-dimethylformamide (DMF) (purity: >99.5%), and ethanol (purity: >99.7%) were purchased from Fuyu Fine Chemical Co. Ltd. (Tianjin, China). N,N′-Dicyclohexylcarbodiimide (DCC) (purity: >99.0%) as a dehydrant and 4-dimethylaminopyridine (DMAP) (purity: >99.0%) as catalysts were purchased from Aladdin Industrial Corporation (Shanghai, China).

2.2. Synthesis of Amino-Functionalized MWCNTs. In a typical process of MWCNTs-COOH, 2 g pristine MWCNTs were mixed with 150 ml acid mixture of concentrated H_2SO_4 and concentrated HNO_3 (volume ratio was 3 : 1). The mixture was treated with ultrasound for 1 hour at ambient temperature (KH-600 KDE, 600 W, 40 kHz) and dispersed evenly. The mixture was then poured into a 250 ml three-neck glass flask, followed by mechanical stirring under 70°C, oil bath for 24 hours. After that, the mixture was diluted with deionized water and precipitated and the supernatant was poured out, diluted, and precipitated multiple times. After centrifugation (TG-16, 8000 rpm, 10 min), we poured off the supernatant and then washed the remaining material with DMF until the pH is 7. Finally, the MWCNTs-COOH was obtained by overnight drying in a vacuum for 60°C.

Amino functional groups are grafted onto carboxylated carbon nanotube. In typical experiments, 0.2 g of MWCNTs-COOH, 20 ml of DMF, 2 g of ODA, 1 g of DCC, and 0.6 g of DMAP were mixed. Then, the mixed liquor was put into trinecked flask and magnetically stirred for 4 days at 100°C oil bath. After that, it was centrifuged (8000 rpm, 10 min) and washed with ethanol and the treated substance was put into a vacuum oven for 60°C (DZF-6020, 450 W, 50 Hz) to dry overnight to get MWCNTs-ODA. The specific synthesis process is shown in Scheme 1.

2.3. Preparation of WMCNTs-ODA/PI Nanocomposite Films. The preparation process of the PI/MWCNTs-ODA composite films includes the synthesis of PAA and preparation of PI. First, 2.2737 g (11.36 mmol) ODA was added in DMAc in a 100 ml trinecked flask, followed by stirring vigorously at room temperature for 30 minutes. Afterwards, 2.5263 g (11.58 mmol) PMDA (the molar ratio of PMDA and ODA was 1.02 : 1) was added in batches for six times, keeping the reaction temperature unchanged. After adding all PMDA, the mixture is kept in ice bath (temperature controlled at 2°C-10°C) for 1 hour. At the same time, 18.5 ml DMAc and a certain amount of prepared MWCNTs-ODA were mixed in the beaker, ultrasonic treatment for 1 hour at room temperature was done for even dispersion, and then MWCNTs-ODA/DMAc mixture was added to the reaction mixture in the ice bath. After the ice bath, the preparation of polyimide precursor polyamic acid (PAA)/MWCNTs-ODA mixture was casted on a clean glass substrate and the thickness was controlled within 1 mm, which was then put into the vacuum oven for 0.5 hour. The mixture underwent a series of thermal treatments afterwards; i.e., it was heated at 30°C for 1 hour, 50°C for 3 hours, 100°C for 1 hour, 200°C for 3 hours, and 250°C for 3 hours to complete the thermal imidization. WMCNTs-ODA/PI was prepared by natural cooling at room temperature. The solid content of

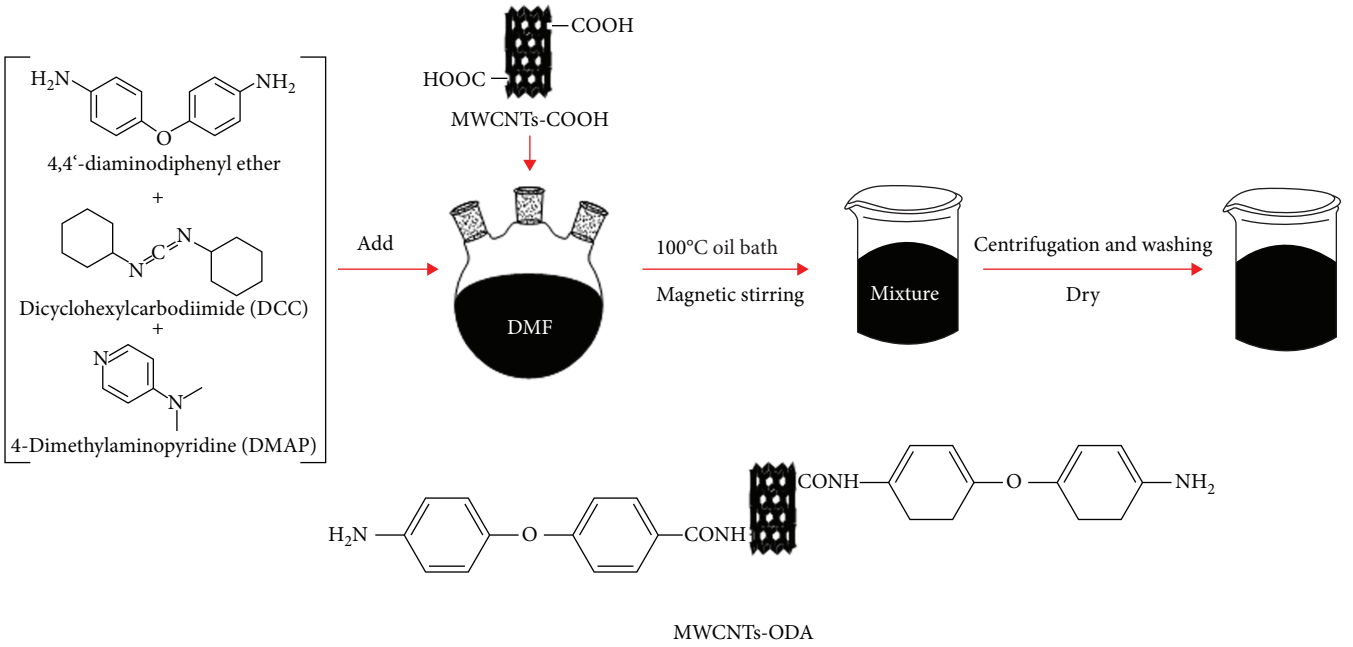

Scheme 1: The preparation process of MWCNTs-ODA.

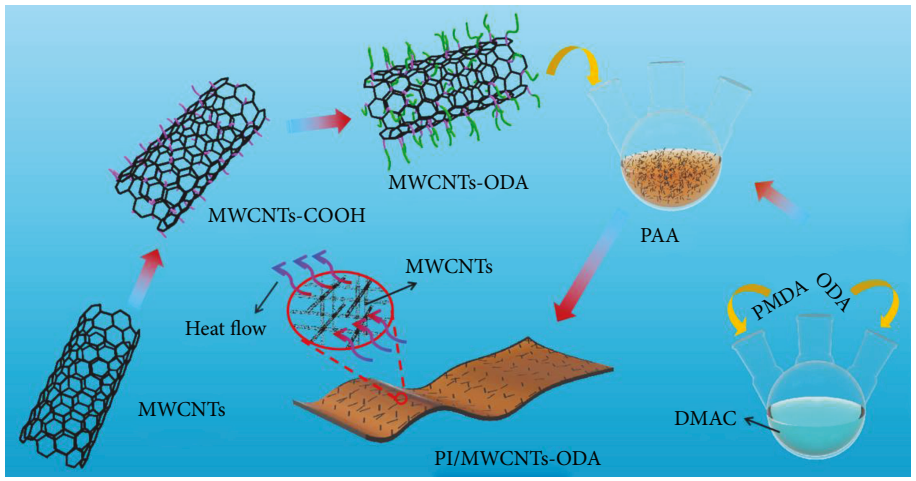

Scheme 2: The preparation process of MWCNTs-ODA/PI composite films.

the composite films was set at 8 wt.%, and the content of MWCNTs-ODA was set at 0 wt.%, 1 wt.%, 1.5 wt.%, 2 wt.%, 2.5 wt.%, 3 wt.%, and 4 wt.%, respectively. The specific synthesis process is shown in Scheme 2.

2.4. Characterization. XRD (X-ray diffraction) patterns of the samples were analyzed by D8 ADVANCE (Bruker Ltd., Germany), employing Cu radiation ($\lambda = 1.5418$ Å). The scanning was performed from 5°-85° at room temperature. FTIR (Fourier Transform infrared spectroscopy) of the samples was recorded by TENSOR II (Bruker Ltd., Germany), scanning from 500 to 4000 cm^{-1}. TEM (transmission electron microscopy) of the samples was analyzed by JEOL JEM-2100 (Japan Electron Optics Laboratory Co. Ltd., Japan). Before the characterizations, the powder samples were dispersed in ethanol and ultrasound was performed for 30-60 minutes. TGA (thermal gravimetric analyses) were conducted on a DSC/TGA Discovery SDT 650 (TA, America) instrument from room temperature to 800°C with a heating rate of 10°C/min in the nitrogen environment. XPS (X-ray photoelectron spectroscopy) of the samples was recorded by ESCALAB 250XI (Thermo Fisher Scientific). Tensile samples were measured by CMT5105 (MTS Corporation, America). The stretching velocity is 500 mm/min, and the sample size is 150 mm × 10 mm × 0.1 mm. SEM (scanning electron microscopy) of the samples was analyzed by Hitachi S-4800 (Hitachi, Japan). The thermal conductivity (λ) of the sample (20 mm × 20 mm × 0.1 mm) was measured by the TPS 2200 Hot Disk instrument (AB Corporation, Sweden). We place the sample between two parallel sensors (3.2 mm diameter), add 0.6 W power heat pulse with the duration of 20 s, and then record the corresponding thermal conductivity. The

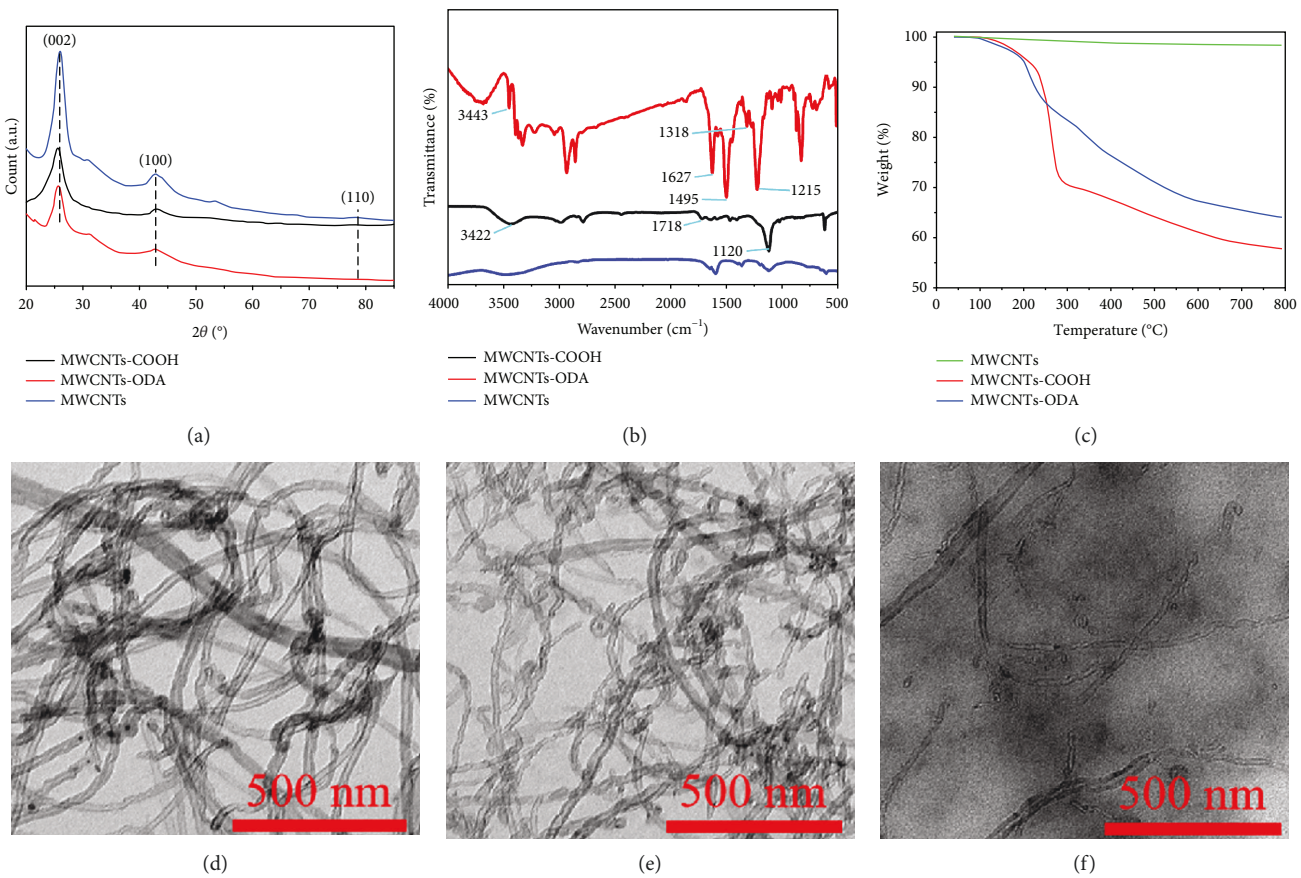

Figure 1: (a) XRD, (b) FTIR, and (c) TGA curves of MWCNTs, MWCNTs-COOH, and MWCNTs-ODA and TEM images of (d) MWCNTs, (e) MWCNTs-COOH, and (f) MWCNTs-ODA.

optical transmittance of composite films was examined by the UV-3600 spectrophotometer (Shimadzu Corporation, Japan); the wavelength range is 200-800 nm.

3. Results and Discussion

3.1. Structure and Performance of MWCNTs, MWCNTs-COOH, and MWCNTs-ODA. The XRD patterns of pure MWCNTs, MWCNTs-COOH, and MWCNTs-ODA are shown in Figure 1(a); it can be seen that the XRD patterns of the pure carbon nanotubes and the modified carbon nanotubes are similar, indicating that the functionalized carbon nanotubes still have the same tubular structure compared with the original carbon nanotubes and the lattice spacing remains unchanged. The pure carbon nanotubes shows strong diffraction peaks at $2\theta = 26^\circ$, 42°, and 77°. The functionalized carbon nanotubes have diffraction peaks at corresponding positions.

The FTIR spectra of pure MWCNTs, MWCNTs-COOH, and MWCNTs-ODA are shown in Figure 1(b); the original carbon nanotubes have no obvious characteristic absorption peaks. In contrast, the MWCNTs-COOH exhibited stretching vibration absorption of C=O and C-O bonds at 1718 cm^{-1} and 1120 cm^{-1} and a characteristic peak of the O-H bond of the carboxyl group appeared at 3422 cm^{-1}. It indicated that the carboxylic acid group was successfully grafted in the surface of the MWCNTs. Due to the formation of the amide bond, a stretching vibration peak of the C=O bond appeared at 1627 cm^{-1}; the characteristic peak at 1318 cm^{-1} is due to the formation of the C-N bond in the amino functional group; the characteristic peak at 1495 cm^{-1} is formed by the C=C bond in the benzene ring; the characteristic peak at 1215 cm^{-1} is formed by the C-O bond in the aromatic ether; and the characteristic peak at 3443 cm^{-1} is due to the N-H bond in the amino functional group. These results suggested that the amino group in the ODA has been successfully grafted onto the CNTs.

The TEM images of pure MWCNTs, MWCNTs-COOH, and MWCNTs-ODA are shown in Figures 1(d)–1(f); the pure CNTs show an obvious agglomeration, and the pipe wall is smooth, with a large aspect ratio and poor dispersion. After introducing the functional group, the aspect ratio of MWCNTs becomes smaller and the dispersion is more uniform, but the tube wall of the CNTs becomes rough. Compared with MWCNTs-COOH, the MWCNTs-ODA have a smaller aspect ratio, a rougher surface, and a significantly improved dispersibility.

The TGA of pure MWCNTs, modified MWCNTs-COOH, and modified MWCNTs-ODA are shown in Figure 1(c); thermogravimetric analysis of functionalized CNTs can provide more detailed information about the thermal stability and surface functionalization. The weight of pure CNTs at 800°C is 98.40%, because the CNTs themselves

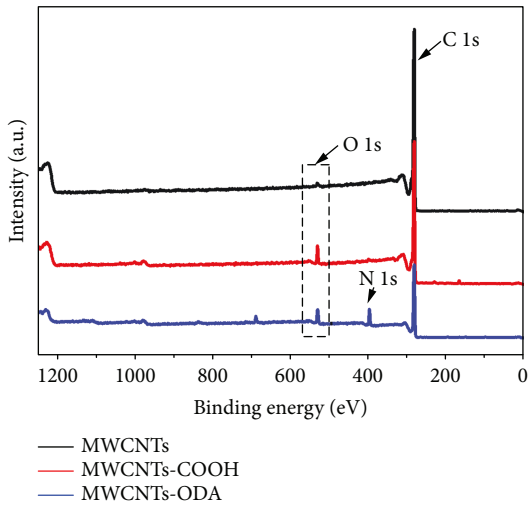

Figure 2: XPS spectrum of MWCNTs, MWCNTs-COOH, and MWCNTs-ODA.

have excellent thermal stability and high temperature resistance, and the weight loss of 1.6% may be due to structural defects of the CNTs themselves. In contrast, carboxylated and aminated CNTs exhibit significant decomposition at lower temperatures. The carboxylated CNTs have a significant weight loss step at 220°C-290°C due to the degradation of carboxyl and hydroxyl groups in MWCNTs-COOH, and the carboxylated CNTs have a residual amount of 57.72% at 800°C. The aminated CNTs have a weight loss of approximately 34.13% in the range of 100°C-700°C; this is mainly due to the thermal decomposition of ODA grafted onto the CNTs. This further demonstrates that ODA is successfully grafted onto the surface of CNTs. In addition, we found that the aminated CNTs have a residual content of 64.07% at 800°C compared to carboxylated CNTs, with higher residuals due to the absence of hydroxyl groups in MWCNTs-ODA, and the benzene ring contained in ODA in MWCNTs-ODA has a stable structure. In other words, replacement of unstable hydroxyl groups in MWCNTs-COOH with more stable ODA groups, MWCNTs-ODA, possesses enhanced thermal stability.

X-ray photoelectron spectroscopy (XPS) analysis was performed to detect the group distribution of the MWCNTs and functionalized MWCNTs. The XPS of pure MWCNTs, modified MWCNTs-COOH, and modified MWCNTs-ODA is shown in Figure 2; the C 1s prominent peak of MWCNTs appeared at 284.8 eV in the test results [49, 50]. Compared with MWCNTs, the O 1s prominent peaks of MWCNTs-COOH and the N 1s prominent peaks of MWCNTs-ODA appeared at 532.6 eV and 399.5 eV, respectively, indicating the presence of O and N atoms in the sample. Among them, MWCNTs-COOH has significantly enhanced O 1s peak intensity compared with MWCNTs. MWCNTs-ODA has new N 1s peaks compared with MWCNTs and MWCNTs-COOH. This all indicates the successful modification of MWCNTs.

The dispersion of DMAc solvent, pure MWCNTs, MWCNTs-COOH, and MWCNTs-ODA is allowed standing for 0 h, 2 h, 4 h, and 8 h, respectively, as shown in Figure 3; we can find that the pure MWCNTs/DMAc mixture showed obvious deposition after standing for 2 h, while the MWCNTs-COOH/DMAc mixture and the MWCNTs-ODA/DMAc mixture dispersed well after standing for 2 h, and there was no obvious deposition appeared. After standing for 4 h and 8 h, the deposition of pure MWCNTs/DMAc mixture became more obvious. The MWCNTs-COOH/DMAc mixture showed deposition after standing for 8 h, while the MWCNTs-ODA/DMAc mixture maintained a very good dispersion. The reason is that after the functionalization of carbon nanotubes, the surface energy can be effectively reduced and the effect of aminated MWCNTs is better, so the dispersibility with organic solvents is better.

3.2. Structural Characterization of the PI and MWCNTs-ODA/PI Composite Films. In order to study the structural characteristics of the pure PI and MWCNTs-ODA/PI composite films, XRD was performed; the result is shown in Figure 4(a). From previous tests, we can know the XRD pattern that the diffraction peak of carbon nanotubes at $2\theta = 26^{\circ}$ is most obvious, while the diffraction peak of PI and MWCNTs-ODA is the same, indicating that the structures of PI chains and MWCNTs do not affect each other. In addition, MWCNTs-ODA has a large lattice spacing, so MWCNTs-ODA has good dispersibility and chemical compatibility in the PI matrix. From the XRD pattern, we found that the XRD of pure PI and MWCNTs-ODA/PI composite films is similar, mainly for two reasons. First, the monomers for synthesizing PI are ODA (diamine) and PMDA (dianhydride). The pure carbon nanotubes are also modified by ODA, so the pure PI and PI composite films contain the same monomer, which is not much different in the XRD pattern. Second, the MWCNTs-ODA content is very small and the performance in XRD is not obvious.

The FTIR was used to detect the chemical bond of the composites [51, 52]. The FTIR spectra of pure PI and MWCNTs-ODA/PI composite films are shown in Figure 4(b); in the FTIR images of pure PI and PI composite films, the characteristic absorption peaks of imide groups appeared at 1778 cm^{-1} and 1707 cm^{-1}, the characteristic peaks of C-N bonds appeared at 1363 cm^{-1}, and the characteristic peaks of C=O bonds appeared at 722 cm^{-1}. It indicated that PI imidization was fully completed. Due to the low content of MWCNTs-ODA in the PI matrix, many functional groups on the surface of MWCNTs-ODA could not be clearly observed in the FTIR results.

3.3. Thermal Properties of the PI and MWCNTs-ODA/PI Composite Films. Thermal stability is an important factor for the application of PI-based composites in high temperature environments [53, 54]. The thermal stability of the films was measured by a TG test under nitrogen atmosphere. The TGA of pure PI and MWCNTs-ODA/PI composite films are shown in Figure 5(a); compared with the work of Kalchounaki et al. [55], the composite film prepared by this work has better thermal stability. The weight loss of the pure PI film at 500°C was 2.1121%, and the residual at 800°C was 55.9794%. It can be seen that the weight loss of the pure PI film and PI/MWCNTs-ODA composite films at 500°C and

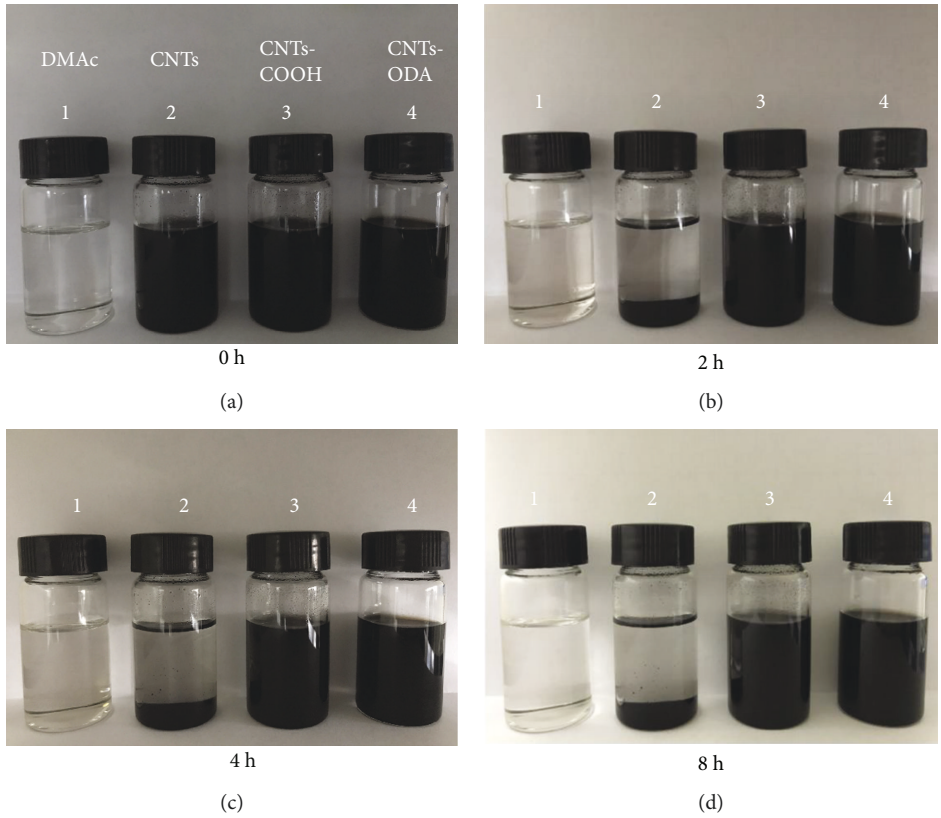

Figure 3: DMAc solvent, pure MWCNTs/DMAc mixture, MWCNTs-COOH/DMAc mixture, and MWCNTs-ODA/DMAc mixture allow standing for (a) 0 h, (b) 2 h, (c) 4 h, and (d) 8 h, respectively.

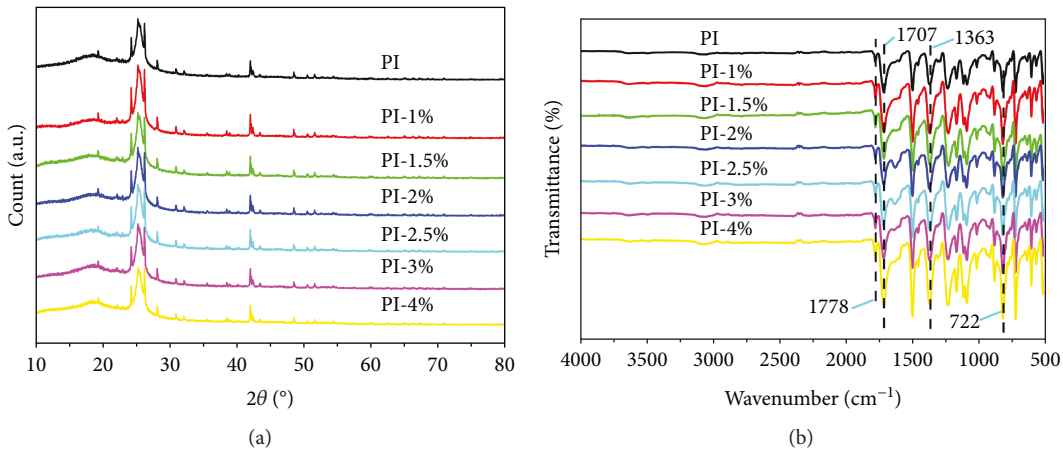

Figure 4: (a) XRD and (b) FTIR curves of pure PI and MWCNTs-ODA/PI composite films.

800°C is not much difference. There are two reasons for this phenomenon: first, only a small amount of aminated carbon nanotubes are added to the PI matrix, so there is no obvious difference in TGA curves; and second, although carbon nanotubes have significant weight loss between 100°C and 700°C after amino functionalization, due to good chemical compatibility and strong interaction between the aminated carbon tubes and the polyimide matrix, when the MWCNTs-ODA content is 3%, the weight loss at 500°C is 1.9077%, When the MWCNTs-ODA content is 3%, the weight loss at 500°C is 1.9077%. The corresponding data of thermal properties are summarized in Table 1.

The thermal conductivity curves of pure PI and MWCNTs-ODA/PI composite films are shown in Figure 5(b); compared with the work of Yan et al. [7], the composite film prepared by this work has better thermal conductivity. When the MWCNTs-ODA content increases from 0 wt.% to 4 wt.%, the thermal conductivity of the PI

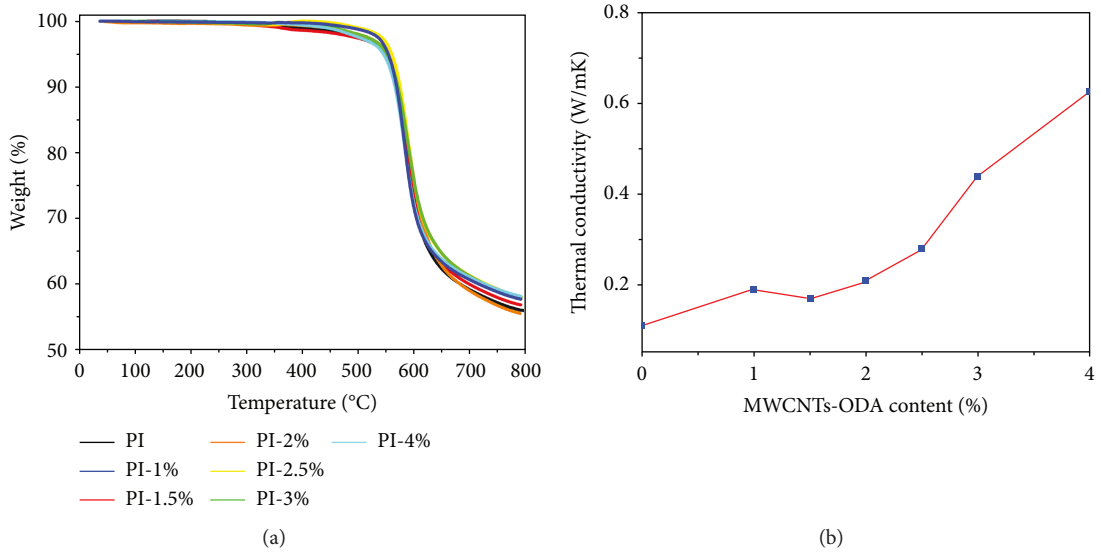

Figure 5: (a) TGA and (b) thermal conductivity curves of pure PI and MWCNTs-ODA/PI composite films.

Table 1: Thermal properties of pure PI and MWCNTs-ODA/PI composite films.

Sample	Thickness (mm)	$T_{5\%}$ (°C)	$T_{10\%}$ (°C)	R_w (%)	References
Pure PI	0.090	553	571	55.9794	
PI-1%	0.073	548	569	57.7443	
PI-1.5%	0.043	554	574	56.8719	
PI-2%	0.075	553	574	55.5747	This work
PI-2.5%	0.049	561	576	58.1314	
PI-3%	0.079	553	573	57.9916	
PI-4%	0.087	546	567	58.2038	
L-GI/MWCNT/PI 5%	—	162	189	46.0000	Kalchounaki et al. [55]

$T_{5\%}$ and $T_{10\%}$: temperature at 5% or 10% weight loss; R_w: residual weight at 800°C.

Table 2: Mechanical properties and thermal conductivity of pure PI and MWCNTs-ODA/PI composite films.

Sample	Pure PI	PI-1%	PI-1.5%	PI-2%	PI-2.5%	PI-3%	PI-4%	MWCNT/PI	BN-c-MWCNT/PI
Tensile strength (MPa)	117.2	126.5	138.4	137.1	140.3	141.5	83.2	135.6	131.9
Thermal conductivity (W/mK)	0.11	0.19	0.17	0.21	0.28	0.44	0.63	0.24	0.38
References	This work							Yan et al. [7]	

The MWCNT and BN-c-MWCNT contents in the reference are both 3 wt.%.

composite film increases with the increase of the MWCNTs-ODA content. Compared with pure PI (0.1366 W/mK), when the WMCNTs-ODA content is 3 wt.%, the thermal conductivity is 0.4397 W/mK. Its thermal conductivity is increased by 221.89%, because when the content of MWCNTs-ODA is low, the CNTs cannot form interconnected heat conduction channels and the carbon nanotubes appear in an isolated state in the PI matrix, which is like an "island-ocean" relationship, so the thermal conductivity is not obviously improved. When the content of carbon nanotubes is increased to 3 wt.%, the thermal conductivity is significantly improved, which is attributed to the fact that the MWCNTs-ODA nanofiller is connected to each other to form a heat conduction channel. The corresponding data of thermal conductivity are summarized in Table 2.

3.4. Mechanical Properties of MWCNTs-ODA/PI Composite Films. The tensile strength of pure PI and MWCNTs-ODA/PI composite films is shown in Figure 6(a); compared with the work of Yan et al. [7], the composite film prepared by this work has better mechanical properties. It can be seen that the tensile strength of the pure PI film is 117.18 MPa. When the MWCNTs-ODA content increased from 0 wt.% to 3 wt.%, the tensile strength of the PI composite films significantly increased, and when the MWCNTs-ODA content was 3 wt.%, the tensile strength reached to 141.48 MPa, compared with pure PI increased by 20.74%. On the one hand, because the MWCNTs-ODA content is below 3 wt.%, the 3D network structure of MWCNTs cross-linking provides the intermolecular bonding force between PI and MWCNTs-ODA. When the composite film is subjected to

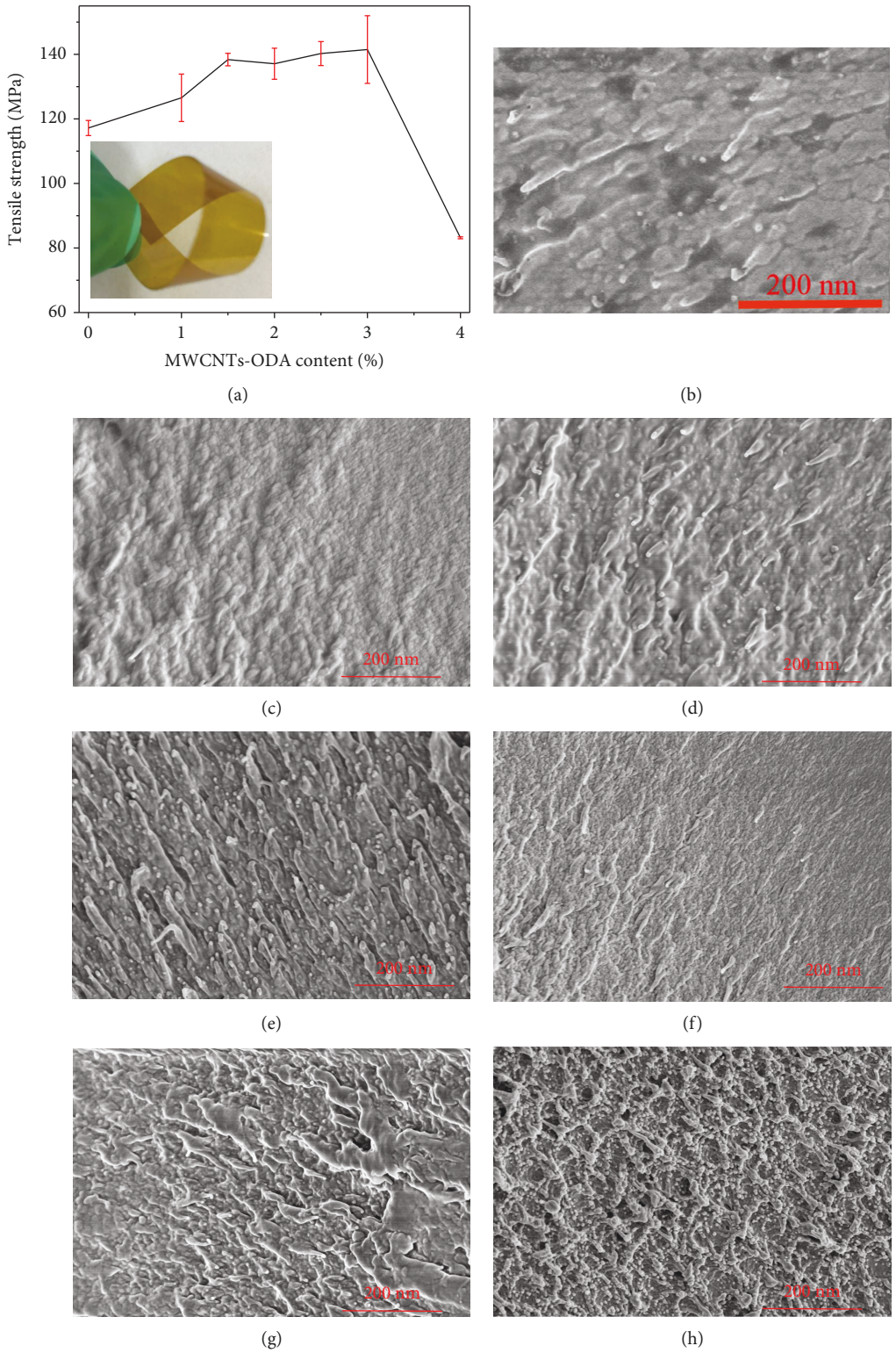

Figure 6: (a) Tensile strength curves of PI composite films and (b–h) SEM images of pure PI and MWCNTs-ODA/PI composite films with the MWCNTs-ODA content of 0 wt.%, 1 wt.%, 1.5 wt.%, 2 wt.%, 2.5 wt.%, 3 wt.%, and 4 wt.%, respectively.

external tensile force, the strong chemical bond between the MWCNTs-ODA and the PI chain can effectively transfer the stress of the PI chain to the surface of the MWCNTs-ODA and thus has excellent mechanical properties. Moreover, due to the good interaction and chemical compatibility between the aminated CNTs and PI matrix, the adhesion between them is obviously enhanced and the mechanical property is improved. However, when the MWCNTs-ODA

content increased from 3 wt.% to 4 wt.%, the tensile strength of the PI composite film decreased significantly, because the additional amount of MWCNTs-ODA reaches the mechanical percolation threshold, and when the MWCNTs-ODA content is lower than this value, the MWCNTs-ODA nanofiller can be well dispersed in the PI matrix and the loading of the composite film can be increased to make the machine works. The performance is significantly improved, and when the MWCNTs-ODA content is higher than this value, the MWCNTs-ODA nanofiller is stacked in the PI matrix, which impairs the improvement of mechanical property. The corresponding data of mechanical properties are summarized in Table 2.

The fracture surface of the tensile test was observed by SEM, and the SEM images of pure PI and 1 wt.%, 1.5 wt.%, 2 wt.%, 2.5 wt.%, 3 wt.%, and 4 wt.% MWCNTs-ODA/PI composite films are shown in Figures 6(b)–6(h), respectively; when the MWCNTs-ODA content is increased from 0 wt.% to 3 wt.%, it can be seen from the SEM image that the cross section of the MWCNTs-ODA/PI composite film has obvious break marks and the composite film is ductile fracture. At this time, the tensile strength of the MWCNTs-ODA/PI composite film increases with the increase of the MWCNTs-ODA content. In addition, when the content of MWCNTs-ODA is 3 wt.%, compared with pure PI, the cross section surface of the PI composite film is rough and there is obvious fracture surface in the enlarged view, due to the excellent interfacial adhesion and well compatibility between the PI matrix and the MWCNTs-ODA nanofiller; it is advantageous to transfer the tensile pressure from the polymer matrix to the MWCNTs-ODA nanofiller. When the MWCNTs-ODA content was increased from 3 wt.% to 4 wt.%, it can be seen from the SEM image that the cross section became significantly rougher and the MWCNTs-ODA/PI composite film was brittle fracture. Correspondingly, the tensile strength of the MWCNTs-ODA/PI composite film showed a significant decrease. Therefore, we conclude that the strong interaction between the nanofiller and the PI matrix makes the MWCNTs-ODA have good dispersibility and this is an important reason for the enhancement of mechanical properties of MWCNTs-ODA/PI nanocomposite films.

3.5. Optical Properties of MWCNTs-ODA/PI Composite Films. The optical properties of MWCNTs-ODA/PI composite films are shown in Figure 7; it shows the optical transmission of the MWCNTs-ODA/PI composite films with a thickness of 43-90 μm in the range of 200-800 nm. The test was carried out with reference to a pure PI film. Due to the introduction of MWCNTs-ODA, the transmittance of composite films decreased from 92.172% (PI-1.5%) to 63.164% (PI-4%), and with the increase of the MWCNTs-ODA content, the color of the films became significantly deeper. The addition of MWCNTs-ODA has a significant effect on the optical properties of MWCNTs-ODA/PI composite films. When the content of MWCNTs-ODA is small, the difference in transmittance of the composite film is not obvious, because the MWCNTs-ODA content is extremely small, resulting in little change in light transmittance.

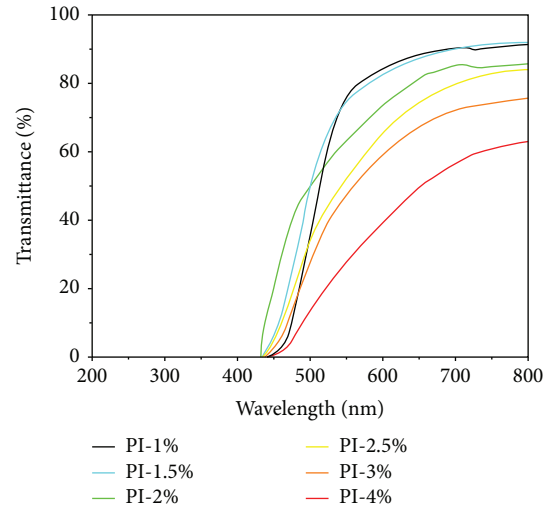

Figure 7: UV-vis spectral curves of PI composite films.

4. Conclusions

In summary, the XRD, FTIR, and XPS tests of MWCNT and MWCNTs-ODA demonstrated that the amino group was successfully grafted on CNTs without destroying the chemical structure of CNTs. The SEM, XRD, and FTIR tests of MWCNTs-ODA/PI composite films confirmed that the addition of MWCNTs-ODA did not destroy the structure and properties of the PI matrix and there was a strong interaction between MWCNTs-ODA and PI matrix and good chemical compatibility between MWCNTs-ODA and PI matrix. Through TGA data of pure PI and MWCNTs-ODA/PI composite films, we found that the addition of MWCNTs-ODA has little effect on the thermal stability of the PI matrix and the composite films has excellent thermal stability, which will not have significant weight loss before 500°C. Through the tensile test of the MWCNTs-ODA/PI composite film, we found that when the MWCNTs-ODA content is 3 wt.%, the tensile strength of the PI composite film is 141.48 MPa, which is 20.74% higher than that of the pure PI film. Through the thermal conductivity test of MWCNTs-ODA/PI composite films, we found that when the content of MWCNTs-ODA is 3 wt.%, the thermal conductivity of the PI composite film is 0.4397 W/mK, which is 221.89% higher than that of the pure PI film. Therefore, when the MWCNTs-ODA content is 3 wt.%, the MWCNTs-ODA/PI composite film has the best comprehensive performance, has excellent thermal conductivity and thermal stability, and might be further used as a potential heat dissipation material in the field of microelectronics and flexible circuit boards. In addition, we also found that as the MWCNTs-ODA content increases, the light transmittance is significantly reduced.

Data Availability

The data used to support the findings of this study are included within the article.

Disclosure

The authors Min Chao and Yanming Li should be considered co-first authors.

Conflicts of Interest

The authors declare that there is no conflict of interest regarding the publication of this paper.

Authors' Contributions

The authors Min Chao and Yanming Li contributed equally to this work.

Acknowledgments

This work was financially supported by the Special Fund for Basic Scientific Research of Central Colleges, Chang'an University (Nos. 300102318403 and 300102319306), the National Science Foundation of China (No. 51407134), the China Postdoctoral Science Foundation (No. 2016M590619), the College Students Innovation and Entrepreneurship Training Program (No. 201810710121), the Natural Science Foundation of Shandong Province (No. ZR2019YQ24), and the Key Laboratory of Engineering Dielectrics and Its Application (Harbin University of Science and Technology), Ministry of Education. The authors also thank their colleagues in their laboratory for their support.

References

[1] Q. Jiang, X. Wang, Y. Zhu, D. Hui, and Y. Qiu, "Mechanical, electrical and thermal properties of aligned carbon nanotube/-polyimide composites," *Composites Part B: Engineering*, vol. 56, pp. 408–412, 2014.

[2] G. Wu, Y. Cheng, Z. Wang, K. Wang, and A. Feng, "In situ polymerization of modified graphene/polyimide composite with improved mechanical and thermal properties," *Journal of Materials Science: Materials in Electronics*, vol. 28, no. 1, pp. 576–581, 2017.

[3] M. Cai, J. Zhu, C. Yang, R. Gao, C. Shi, and J. Zhao, "A parallel bicomponent TPU/PI membrane with mechanical strength enhanced isotropic interfaces used as polymer electrolyte for lithium-ion battery," *Polymers*, vol. 11, no. 1, p. 185, 2019.

[4] M. Chao, "Synthesis and characterization of semicrystalline polyimides containing bridged linkages," *International Journal of Polymer Science*, vol. 2018, Article ID 8590567, 7 pages, 2018.

[5] Z. Ahmad and J. E. Mark, "Polyimide-ceramic hybrid composites by the sol-gel route," *Chemistry of Materials*, vol. 13, no. 10, pp. 3320–3330, 2001.

[6] S. Jiang, H. Hou, S. Agarwal, and A. Greiner, "Polyimide nanofibers by "green" electrospinning via aqueous solution for filtration applications," *ACS Sustainable Chemistry & Engineering*, vol. 4, no. 9, pp. 4797–4804, 2016.

[7] W. Yan, Y. Zhang, H. Sun et al., "Polyimide nanocomposites with boron nitride-coated multi-walled carbon nanotubes for enhanced thermal conductivity and electrical insulation," *Journal of Materials Chemistry A*, vol. 2, no. 48, pp. 20958–20965, 2014.

[8] J. Dong, C. Yin, X. Zhao, Y. Li, and Q. Zhang, "High strength polyimide fibers with functionalized graphene," *Polymer*, vol. 54, no. 23, pp. 6415–6424, 2013.

[9] X. Xue, H. Yan, and Y. Fu, "Preparation of pure and metal-doped $Li_4Ti_5O_{12}$ composites and their lithium-storage performances for lithium-ion batteries," *Solid State Ionics*, vol. 335, pp. 1–6, 2019.

[10] Z. Li, K. Kou, J. Xue, C. Pan, and G. Wu, "Study of triazine-based-polyimides composites working as gel polymer electrolytes in ITO-glass based capacitor devices," *Journal of Materials Science: Materials in Electronics*, vol. 30, no. 4, pp. 3426–3431, 2019.

[11] W. Dai, J. Yu, Z. Liu et al., "Enhanced thermal conductivity and retained electrical insulation for polyimide composites with SiC nanowires grown on graphene hybrid fillers," *Composites Part A: Applied Science and Manufacturing*, vol. 76, pp. 73–81, 2015.

[12] L. Zuo, W. Fan, Y. Zhang et al., "Graphene/montmorillonite hybrid synergistically reinforced polyimide composite aerogels with enhanced flame-retardant performance," *Composites Science and Technology*, vol. 139, pp. 57–63, 2017.

[13] Y. Qin, Q. Peng, Y. Ding et al., "Lightweight, superelastic, and mechanically flexible graphene/polyimide nanocomposite foam for strain sensor application," *ACS Nano*, vol. 9, no. 9, pp. 8933–8941, 2015.

[14] T. Zhang, Y. Zhao, and K. Wang, "Polyimide aerogels cross-linked with aminated Ag nanowires: mechanically strong and tough," *Polymers*, vol. 9, no. 12, p. 530, 2017.

[15] Y. Song, H. Yao, H. Tan et al., "Synthesis and memory characteristics of highly organo-soluble hyperbranched polyimides with various electron acceptors," *Journal of Polymer Science Part A: Polymer Chemistry*, vol. 55, no. 14, pp. 2281–2288, 2017.

[16] X. Li, J. Wang, Y. Zhao, and X. Zhang, "Template-free self-assembly of fluorine-free hydrophobic polyimide aerogels with lotus or petal effect," *ACS Applied Materials & Interfaces*, vol. 10, no. 19, pp. 16901–16910, 2018.

[17] X. Lei, M. Qiao, L. Tian, Y. Chen, and Q. Zhang, "Tunable permittivity in high-performance hyperbranched polyimide films by adjusting backbone rigidity," *The Journal of Physical Chemistry C*, vol. 120, no. 5, pp. 2548–2561, 2016.

[18] S. Han, J. T. Lin, Y. Yamada, and D. D. L. Chung, "Enhancing the thermal conductivity and compressive modulus of carbon fiber polymer–matrix composites in the through-thickness direction by nanostructuring the interlaminar interface with carbon black," *Carbon*, vol. 46, no. 7, pp. 1060–1071, 2008.

[19] C. K. Leong, Y. Aoyagi, and D. D. L. Chung, "Carbon black pastes as coatings for improving thermal gap-filling materials," *Carbon*, vol. 44, no. 3, pp. 435–440, 2006.

[20] X. Liang, Y. Yang, X. Jin, Z. Huang, and F. Kang, "The high performances of SiO_2/Al_2O_3-coated electrospun polyimide fibrous separator for lithium-ion battery," *Journal of Membrane Science*, vol. 493, pp. 1–7, 2015.

[21] H. Wang, H. Li, L. Yu, Y. Jiang, and K. Wang, "Synthesis of porous Al_2O_3-PVDF composite separators and their application in lithium-ion batteries," *Journal of Applied Polymer Science*, vol. 130, no. 4, pp. 2886–2890, 2013.

[22] Y. Zhou, H. Wang, L. Wang et al., "Fabrication and characterization of aluminum nitride polymer matrix composites with high thermal conductivity and low dielectric constant for electronic packaging," *Materials Science and Engineering: B*, vol. 177, no. 11, pp. 892–896, 2012.

[23] B. L. Zhu, J. Wang, J. Ma, J. Wu, K. C. Yung, and C. S. Xie, "Preparation and properties of aluminum nitride-filled epoxy composites: effect of filler characteristics and composite processing conditions," *Journal of Applied Polymer Science*, vol. 127, no. 5, pp. 3456–3466, 2013.

[24] Y. Zhou, L. Wang, H. Zhang, Y. Bai, Y. Niu, and H. Wang, "Enhanced high thermal conductivity and low permittivity of polyimide based composites by core-shell Ag@SiO2 nanoparticle fillers," *Applied Physics Letters*, vol. 101, no. 1, article 012903, 2012.

[25] M. Shanthil, R. Thomas, R. S. Swathi, and K. George Thomas, "$Ag@SiO_2$ core–shell nanostructures: distance-dependent plasmon coupling and SERS investigation," *The Journal of Physical Chemistry Letters*, vol. 3, no. 11, pp. 1459–1464, 2012.

[26] G. Wu, J. Li, K. Wang, Y. Wang, C. Pan, and A. Feng, "In situ synthesis and preparation of TiO_2/polyimide composite containing phenolphthalein functional group," *Journal of Materials Science: Materials in Electronics*, vol. 28, no. 9, pp. 6544–6551, 2017.

[27] Z. Yuan, J. Yu, B. Rao et al., "Enhanced thermal properties of epoxy composites by using hyperbranched aromatic polyamide grafted silicon carbide whiskers," *Macromolecular Research*, vol. 22, no. 4, pp. 405–411, 2014.

[28] Y. Niu, X. Zhang, J. Zhao, Y. Tian, Y. Li, and X. Yan, "Preparation, characterization and properties of amine-functionalized silicon carbide/polyimide composite films," *RSC Advances*, vol. 4, no. 54, article 28456, 2014.

[29] W. Zhou, C. Wang, T. Ai, K. Wu, F. Zhao, and H. Gu, "A novel fiber-reinforced polyethylene composite with added silicon nitride particles for enhanced thermal conductivity," *Composites Part A: Applied Science and Manufacturing*, vol. 40, no. 6-7, pp. 830–836, 2009.

[30] Y. Zhou, H. Hyuga, D. Kusano, Y. Yoshizawa, and K. Hirao, "A tough silicon nitride ceramic with high thermal conductivity," *Advanced Materials*, vol. 23, no. 39, pp. 4563–4567, 2011.

[31] J. Hou, G. Li, N. Yang et al., "Preparation and characterization of surface modified boron nitride epoxy composites with enhanced thermal conductivity," *RSC Advances*, vol. 4, no. 83, pp. 44282–44290, 2014.

[32] K. Sato, H. Horibe, T. Shirai et al., "Thermally conductive composite films of hexagonal boron nitride and polyimide with affinity-enhanced interfaces," *Journal of Materials Chemistry*, vol. 20, no. 14, p. 2749, 2010.

[33] S. Uchida, T. Murakami, T. Iwamura, R. Ishige, and S. Ando, "Enhanced thermal conductivity in immiscible polyimide blend composites with needle-shaped ZnO particles," *RSC Advances*, vol. 7, no. 25, pp. 15492–15499, 2017.

[34] D. Yorifuji and S. Ando, "Enhanced thermal conductivity over percolation threshold in polyimide blend films containing ZnO nano-pyramidal particles: advantage of vertical double percolation structure," *Journal of Materials Chemistry*, vol. 21, no. 12, p. 4402, 2011.

[35] P. Kim, L. Shi, A. Majumdar, and P. L. McEuen, "Thermal transport measurements of individual multiwalled nanotubes," *Physical Review Letters*, vol. 87, no. 21, article 215502, 2001.

[36] R. H. Baughman, C. Cui, A. A. Zakhidov et al., "Carbon nanotube actuators," *Science*, vol. 284, no. 5418, pp. 1340–1344, 1999.

[37] M. J. Esplandiu, V. G. Bittner, K. P. Giapis, and C. P. Collier, "Nanoelectrode scanning probes from fluorocarbon-coated single-walled carbon nanotubes," *Nano Letters*, vol. 4, no. 10, pp. 1873–1879, 2004.

[38] M. Cadek, J. N. Coleman, K. P. Ryan et al., "Reinforcement of polymers with carbon nanotubes: the role of nanotube surface area," *Nano Letters*, vol. 4, no. 2, pp. 353–356, 2004.

[39] C. Wei, D. Srivastava, and K. Cho, "Thermal expansion and diffusion coefficients of carbon nanotube-polymer composites," *Nano Letters*, vol. 2, no. 6, pp. 647–650, 2002.

[40] K. Wang, Y. H. Chang, C. Zhang, and B. Wang, "Conductive-on-demand: tailorable polyimide/carbon nanotube nanocomposite thin film by dual-material aerosol jet printing," *Carbon*, vol. 98, pp. 397–403, 2016.

[41] L. Yan, G. Zhang, L. Zhang et al., "Robust construction of underwater superoleophobic CNTs/nanoparticles multifunctional hybrid membranes via interception effect for oily wastewater purification," *Journal of Membrane Science*, vol. 569, pp. 32–40, 2019.

[42] S. Song, Y. Zhai, and Y. Zhang, "Bioinspired graphene oxide/-polymer nanocomposite paper with high strength, toughness, and dielectric constant," *ACS Applied Materials & Interfaces*, vol. 8, no. 45, pp. 31264–31272, 2016.

[43] Z. Wang, X. Shen, M. Akbari Garakani et al., "Graphene aerogel/epoxy composites with exceptional anisotropic structure and properties," *ACS Applied Materials & Interfaces*, vol. 7, no. 9, pp. 5538–5549, 2015.

[44] W. H. Liao, S. Y. Yang, J. Y. Wang et al., "Effect of molecular chain length on the mechanical and thermal properties of amine-functionalized graphene oxide/polyimide composite films prepared by in situ polymerization," *ACS Applied Materials & Interfaces*, vol. 5, no. 3, pp. 869–877, 2013.

[45] J. F. Wang, X. X. Jin, H. Wu, and S. Y. Guo, "Polyimide reinforced with hybrid graphene oxide @ carbon nanotube: toward high strength, toughness, electrical conductivity," *Carbon*, vol. 123, pp. 502–513, 2017.

[46] X. L. Li, J. L. Lan, M. Ai, Y. G. Guo, Q. Cai, and X. P. Yang, "Biomineralization on polymer-coated multi-walled carbon nanotubes with different surface functional groups," *Colloids and Surfaces B: Biointerfaces*, vol. 123, pp. 753–761, 2014.

[47] X. H. Chen, J. F. Wang, M. Lin et al., "Mechanical and thermal properties of epoxy nanocomposites reinforced with amino-functionalized multi-walled carbon nanotubes," *Materials Science and Engineering: A*, vol. 492, no. 1-2, pp. 236–242, 2008.

[48] Y. Chen, D. X. Li, W. Y. Yang, C. G. Xiao, and M. L. Wei, "Effects of different amine-functionalized graphene on the mechanical, thermal, and tribological properties of polyimide nanocomposites synthesized by in situ polymerization," *Polymer*, vol. 140, pp. 56–72, 2018.

[49] H. Yan, Y. Fu, X. Wu, X. Xue, C. Li, and L. Zhang, "Core-shell structured $NaTi_2(PO_4)_3$@polyaniline as an efficient electrode material for electrochemical energy storage," *Solid State Ionics*, vol. 336, pp. 95–101, 2019.

[50] H. Zhang, B. Wang, A. Feng et al., "Mesoporous carbon hollow microspheres with tunable pore size and shell thickness as efficient electromagnetic wave absorbers," *Composites Part B: Engineering*, vol. 167, pp. 690–699, 2019.

[51] J. Li, J. Ma, S. Chen, J. He, and Y. Huang, "Characterization of calcium alginate/deacetylated konjac glucomannan blend films prepared by Ca^{2+} crosslinking and deacetylation," *Food Hydrocolloids*, vol. 82, pp. 363–369, 2018.

[52] J. Li, J. Ma, S. Chen, Y. Huang, and J. He, "Adsorption of lysozyme by alginate/graphene oxide composite beads with

enhanced stability and mechanical property," *Materials Science and Engineering C*, vol. 89, pp. 25–32, 2018.

[53] Z. Wang, M. Yang, Y. Cheng et al., "Dielectric properties and thermal conductivity of epoxy composites using quantum-sized silver decorated core/shell structured alumina/polydopamine," *Composites: Part A*, vol. 118, pp. 302–311, 2019.

[54] A. Feng, G. Wu, C. Pan, and Y. Wang, "Synthesis, preparation and mechanical property of wood fiber-reinforced poly(vinyl chloride) composites," *Journal of Nanoscience and Nanotechnology*, vol. 17, no. 6, pp. 3859–3863, 2017.

[55] E. K. Kalchounaki, A. Farhadi, and A. Zadehnazari, "Preparation and properties evaluation of polyimide-matrix nanocomposites reinforced with glutamine functionalized multi-walled carbon nanotube," *Polymer Bulletin*, vol. 75, no. 12, pp. 5731–5744, 2018.